Bubble assisted vacuum thermoforming: considerations to extend the use of in-situ stereo-DIC measurements to stretching of sagged thermoplastic sheets

Abderrahmane Ayadi, Marie-France Lacrampe, Patricia Krawczak

Bubble assisted vacuum thermoforming: considerations to extend the use of in-situ stereo-DIC measurements to stretching of sagged thermoplastic sheets

A. Ayadi[1,2] & M.-F. Lacrampe[1,2] & P. Krawczak[1,2]

In bubble assisted vacuum thermoforming, measuring pressure-induced mechanical strains through the stereo-digital image correlation (stereo-DIC) technique while shaping thermoplastic sheet requires consideration of an appropriate reference state of surface deformations. However, when the stereoscopic measurements can be only performed after the heating step, the correlation problem should be well-posed otherwise the reliability of results is limited. This study focuses on stretching by bubble inflation processes following thermal warpage and sagging of initially flat sheets. For this purpose, an experimental rig is instrumented to heat high impact polystyrene (HIPS) sheets and to perform synchronized pressure and stereoscopic measurements during 1.5 s stretching. A two-step method is introduced to separate mechanical strains which are affected by the uncontrollable change of initial conditions from the global stereo-DIC strains. The first step relies on amplification of damped oscillations at the initiation of the inflation process due to sagging. Out-of-plane displacements confirm the existence of a temperature-dependent characteristic time that marks the transition from the sagged to the strained surface shapes. The second step uses these characteristic times to objectively shift the reference of image-correlation computations. To evaluate the effectiveness of the suggested method, inaccuracy levels of global strains are evaluated at a fixed pressure level under different thermal conditions. It is shown that inaccuracy levels are the highest when stereo-DIC measurements followed warpage and they decrease with amplification of sagging. The developed approach extends the use of in-situ stereo-DIC measurements when changes of initial conditions are uncontrollable and thermal strains cannot be measured.

Keywords Thermoforming · Stretching · Thin thermoplastic sheets · Sag · Principal strains · In-situ stereo DIC

Introduction

In bubble-assisted thermoforming processes, deforming thin thermoplastic sheets to obtain parts of 3D geometries follows a sequence of successive steps which include clamping, heating and stretching. The first two steps impose the required thermal and mechanical conditions which guarantee large deformations of the thermoplastic without breakage nor catastrophic thinning [1–4]. The stretching step generally takes place between the end of the heating step and before bringing the sheet into contact with the walls of a mold. It corresponds to a dynamic inflation process during which pressurized air is introduced within less than a few seconds inside a closed volume which is sealed by the thermoplastic sheet [5, 6]. The fast increase of the pressure-difference between the inside and the outside of the closed volume forces the thermoplastic which is at the rubbery state to form a bubble-like-shape [7, 8]. This fast operation is featured by the insignificance of viscous effects, the dependence of the large mechanical deformations on the driving pressure and the potential occurrence of geometric instabilities [9–11]. In the case of spherical thin sheets *Verron et al.* demonstrated that these geometric instabilities are associated with a sudden jump of the

✉ M.-F. Lacrampe
marie-france.lacrampe@imt-lille-douai.fr

[1] Institut Mines-Télécom, Polymers and Composites Technology & Mechanical Engineering Department, IMT Lille Douai, 941 rue Charles Bourseul, 59508 Douai, France

[2] Université de Lille, 59000 Lille, France

pressure at the initiation of the dynamic inflation process and manifest as damped oscillations between an initially unconstrained state of the sheet and around a quasi-static equilibrium state [12, 13].

In experimental mechanics, stereo digital image correlation (stereo-DIC) is a non-contact technique which provides full-fields of displacements and strains. It combines two fundamental functions: stereo-vision and image correlation [14–16]. During an experimental test, a system of stereo cameras records images of a speckle pattern applied on the surface before deforming a sample. The images from different observation angles are then correlated to match image subsets between the cameras. The changes in 3D surface geometry throughout the deformation are then obtained through triangulation and correlation of each deformed image pair with the reference pair. This process provides the 3D positions within the referential of the stereo-vision system of each material point located on the deformed surface from which 3D displacement vectors are calculated [17, 18]. Recently, *Van Mieghem et al.* confirmed the reliability of stereo-DIC to measure large strains during thermoforming of high impact polystyrene (HIPS) sheets [19]. Because thermoforming is a multi-step process, the sheet deformations were recorded starting from the clamping step and the reference of correlation computations was attributed to the initially flat surface of the sheet. Thus, the obtained full-fields of strains at the end of the thermoforming cycle represented cumulated thermal induced and mechanical strains [20, 21].

Assessment of mechanical strains during the stretching step, requires separation of thermal strains from the global stereo-DIC strains or direct stereo-DIC measurements during the dynamic inflation process. However, both operations are not always feasible due to three major issues. The first issue is related to the technology of the thermoforming equipment which may inhibit the accessibility of the stereo-vision system to the sheet during the heating step. Consequently, thermal strains cannot be measured. The second issue is related to the uncontrollable change of initial conditions between the start and the end of the heating step. In fact, thermoplastic sheets are generally heated to a forming temperature window by exposing them to infra-red (IR) heaters. During the stabilization of the temperature between the heat deflection (T_{HD}) and melting temperatures, inevitable flaws such as warpage and sag may occur and induce stochastic out-of-plane deformations of the initially flat sheet. Warpage manifests due to the relaxation of residual stresses which are related to the processing history of the used sheet (mainly extrusion or calendaring processes) [22–24]. By exceeding the T_{HD} threshold, the tensile strength decreases, viscous effects become significant, and hence the softened sheet stretches under the effect of the gravity force [25]. This phenomenon taking place during the heating step is known by sagging [26, 27]. The third issue corresponds to errors of the stereo-DIC technique. *Murienne et al.* classified them into errors of reconstruction sources and those of correlation sources [28]. While reconstruction errors are related to the calibration of the stereo-vision system, correlation errors are often related to large out-of-plane deformations. In the case of large rigid body translations and rotations, *Sutton et al.* demonstrated that correlation errors are negligible and that stereo-vision systems are able to accurately measure all components of displacement vectors [29]. In the case of non-linear large deformations, numerous studies provided theoretical and experimental methods to accurately measure the out-of-plane components of displacement vectors and to evaluate effective mechanical strains [30, 31]. Recently, *Rokos et al.* demonstrated that the choice of the reference state of correlation computations also constitutes a critical source of strain errors. Accurate choice of the reference state is mostly considered for integrated digital image correlation experiments where the boundary conditions of the mechanical problem are defined outside the considered field-of-view of the stereo-vision system. The authors concluded if such a choice does not take into consideration the changes of boundary conditions during the experimental test, then the digital image correlation problem is ill-posed and the correlation results are erroneous [32].

The aim of the current study is to suggest an experimental approach which evaluates pressure induced mechanical strains during dynamic inflation of sagged thermoplastic sheets such as the thermal induced changes of initial conditions cannot be followed by the stereo-vision system. The suggested approach is based on the separation of the stretching step into two sub-steps: a first sub-step which covers the required duration for the attenuation of damped oscillations at the initiation of the dynamic inflation operation and a second sub-step which covers the quasi-stable stretching of the sheet. For this purpose, relatively fast stereo-vision measurements are performed to monitor the attenuation of out-of-plane instabilities following four different heating conditions. Then, the corresponding time-evolution are identified using a decayed exponential fitting to objectively shift the reference state of image correlation computations to the moment of attenuation of the damped oscillations. The computed principal strains before and after shifting the reference state are used to separate between mechanical strains corresponding to each of the considered sub-steps. The medians of mechanical strains at the end of the damped oscillations will be considered to evaluate the effect of the heating temperatures on the global stereo-DIC strains measured during the stretching step.

Materials and methods

Materials

The experimental work was conducted on monolayer and flat sheets of HIPS (*Athpol P91®; Ireland). T*his considered thermoplastic grade is characterized by a temperature of heat deflection (T_{HD}) of 90 °C and a density of 1.05 g/cm^3 (Table 1). The used samples had a rectangular geometry of 600 × 330 mm^2 and a uniform thickness of 1.5 mm. To reduce the scatter of mechanical measurements potentially induced by the aspect ratio (which equal to 1.8) of the considered geometry, a common cutting orientation was respected. As required for stereo-DIC measurements, random speckle patterns were applied on the top side of each of the samples by respectively applying a thin layer of a mat white paint and then spraying black paint on top of it.

Experimental rig

Dynamic bubble inflation

To regenerate damping surface oscillations an industrial thermoforming equipment (*UA-100Ed, Illig®, Germany*) is used. The machine is equipped with a positive mold which is located inside the forming cabinet and connected to an electric valve which controls the inlet of the pressurized-air circuit. The commanding part provides the possibility to define automatic forming cycles based on configuration of a set of predefined steps. In the current study, the considered forming sequence comprises clamping (2 s), heating (70 s) and stretching (1.5 s) steps.

The cycle starts by applying a mechanical pressure on the edges (Γ_{sheet}) of the HIPS sheet (Ω_{sheet}) by using a wooden clamp-frame that contains a circular opening of 250 mm in diameter (Fig. 1a and b). At the end of the clamping step, the forming cabined is sealed and the internal pressure is kept equal to the atmospheric pressure P_{atm}. With consideration of a material point (M) of coordinates (X,Y,0) and located at the top surface of the HIPS sheet, the initial boundary conditions can be summarized as expressed in eq. (1):

$$M\in\overline{\Omega_{sag}};\begin{cases}T_M\ll T_{HD};\\ w_M=0;\end{cases}\ and\ M\in\Gamma_{sheet};\begin{cases}u_M=v_M=w_M=0;\\ rx_M=ry_M=rz_M=0;\end{cases}\quad(1)$$

Where, $\overline{\Omega_{sag}}$ is the domain of the sheet located outside the opening of the clamp frame; T_M is the temperature of at the position of the material point M; u_M; v_M and w_M (respectively rx_M; ry_M and rz_M) are displacement (and rotation) degrees of freedom within the directions of the common referential (X, Y, Z) of the stereo-vision system.

During the heating step, an IR-heater parallel to the top surface of the sheet covers the whole the clamp frame from a distance of 150 mm (Fig. 1c). Only the domain Ω_{sag} is exposed to the heater and the heat transfer problem is limited to radiative heating at the exposed surface (at Z = 0 mm) and conduction heating through the limited thickness. Temperature dissipation is limited to negligible convection with the air inside the sealed forming. In literature numerous studies have studied the heating step in thermoforming [33, 34]. Thus, the general time dependent conduction-convection-radiation problem can be simplified as expressed in the system of eqs. (2):

$$M\in\Omega_{sag};\begin{cases}\rho C_p\dfrac{\partial T}{\partial t}=k\ \nabla^2 T;\\ k\dfrac{\partial T}{\partial z}\ (z=0,t>0)=\lambda\left(T_{heater}^4-T^4\right);\\ -k\dfrac{\partial T}{\partial z}\ (z=-1.5,t>0)=h(T_{air}-T);\end{cases}\quad(2)$$

Where,

- t is the heating time;
- T is the absolute temperature;
- k is the plastic thermal conductivity;
- h is the convection parameter and
- λ is a constant which incorporates geometric parameters and radiant properties of the heater and the sheet.

Because the main interest of this study is related to the stretching step, the temperature control was limited to experimental measurements of the temperature of the heated surface of the sheet. To amplify the sheet buckling caused by sagging, the heating duration was extended up to 70 s. At the end of the heating step, the conditions of the can be simplified as indicated in the system of eqs. (3):

$$M\in\Omega_{sag};\begin{cases}T_M\geq T_{HD}\\ \overrightarrow{F}=-m\times\overrightarrow{g}\\ w_M(t)\leq 0;\end{cases}\quad(3)$$

Where, m is the mass of the Ω_{sag} domain and $\overrightarrow{g}$ is a constant vector of magnitude of 9.81 m/s^2.

Table 1 List of the thermal and mechanical properties of the used HIPS grade (supplier data)

Properties	Values	Units
Heat Deflection Temperature (at 1.8 MPa)	90	°C
Density	1.05	g/cm^3
Thermal conductivity	0.17	W/mK
Specific Heat	1200	J/kgK

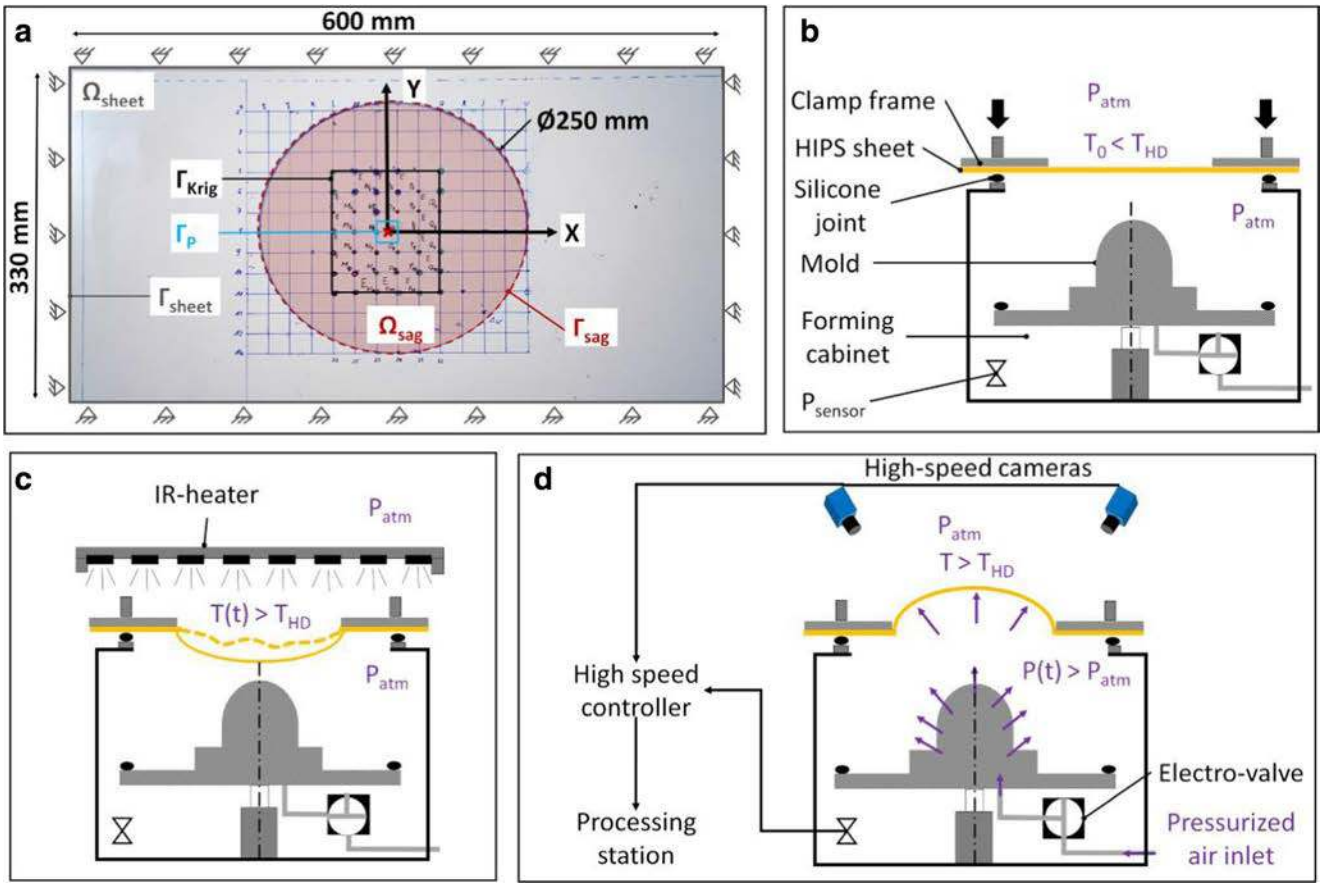

Fig. 1 **a** Considered domains of interest (Ω) and applied initial boundary conditions on the edges of the sheet (Γ_{sheet}). **b-c-d** Schematic representation of the respective clamping, heating and stretching steps

The third and final step starts at the moment of the complete retraction of the IR-heater and corresponds to a dynamic inflation process of 1.5 s (Fig. 1d). The electric valve is automatically opened to introduce pressurized-air within the sealed forming cabined through air vents of the mold. First, the pressure increase forces the sagged domain Ω_{sag} to exhibit damped oscillation for a limited duration τ_T and then to stretch by forming a bubble-like-shape of 250 mm in diameter. The sheet's inertia during dynamic inflation processes can be assimilated to the inflation of a material of a rubber-like-behavior submitted to constant air flow [13].

Synchronized control of pressure and surface deformations

The used experimental rig was instrumented by a sensor (*AP-30, JUMO®, France*) to record relative pressure inside the forming cabinet during the stretching step of the HIPS sheet and by a stereo-DIC system (*LaVision®, Germany*) to record the surface deformations. As illustrated in Fig. 1**d**, the pressure sensor was positioned inside the sealed forming cabinet and a pair of high-speed cameras (*Imager MX 4 M, LaVision®, Germany*) were positioned on the top of the thermoforming equipment. The pressure signal and image recording were synchronized via a high-speed-controller that was commanded via the software *DaVis v8.4* (*LaVision®, Germany)*. With respect of the same technical considerations that were used in a previous work of the authors [1], relative pressure and full-resolution images (2048 × 2048 pixels) were simultaneously recorded at a frequency of 180 Hz during almost 3 s starting from the automatic onset of the retraction of the IR heater. Figure 2 provides an indication about the synchronized recording of pressure signal with pairs of stereo-images.

Calibration operations

Stereo-DIC calibration

In general, the stereo-DIC technique associates stereoscopic measurements with an image correlation method to evaluate 3D vectors including displacements and strains. To evaluate the intrinsic parameters of the stereoscopic system (formed by at least two cameras) and compensate the effect of optical imprecisions a calibration procedure was conducted by using a reference plate (*309–15-SSDP, LaVision®, Germany)* and the software *DaVis v8.4*. A total of six pairs of images from

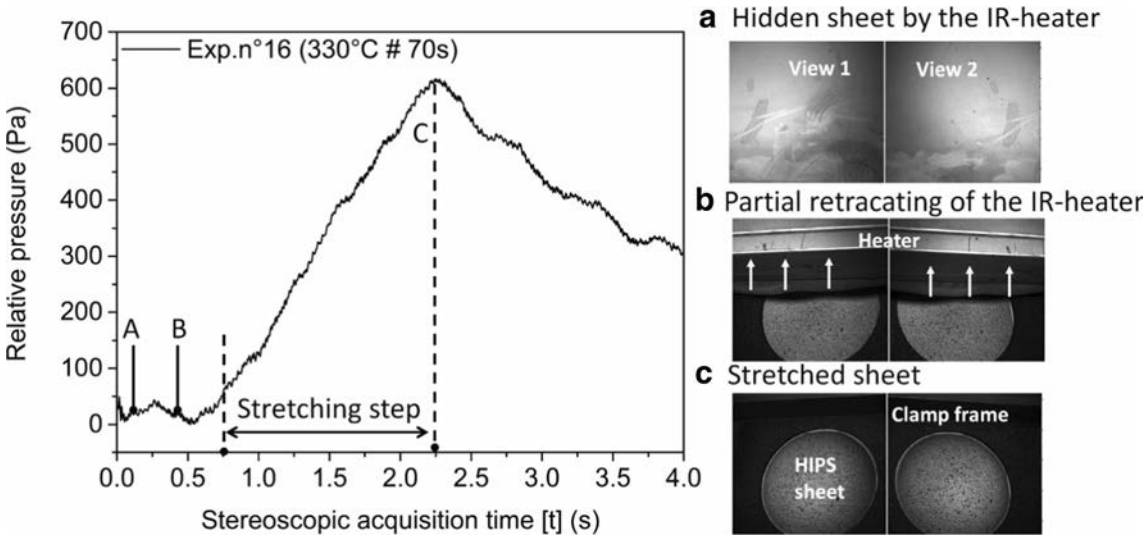

Fig. 2 (Left) Recorded pressure signal during a stretching operation conducted after a heating step (at 330 °C during 70 s). (Right) Pairs of stereo images corresponding to the moments indicated by the letters A, B and C

different positions was required to cover a region of interest of $200 \times 200 \times 100$ mm^3 including the spatial domain where the HIPS sheet was expected to evolve. Then, for each of the recorded images the coordinates of characteristic markers that were on the surface of the used calibration plate were extracted. The obtained coordinates served as input data to a pinhole model [35] to evaluate the intrinsic parameters of the used stereoscopic system and to define a common coordinates system. Table 2 summarizes the parameters obtained at the end of the calibration procedure.

Thermal conditions and surface planarity change

Because of the variability of thermoforming parameters, the conducted experimental work relied on changing the regulation-temperature of the IR heater and fixing all other parameters (notably the pressurized-air flow, the air inflation duration and the heating duration). However, to control the heights of the formed domes during stretching a two-step calibration procedure of thermal conditions was also required. The first step was based on trial tests with respected of two technical constraints: first, the lowest limit of the regulation temperatures should not prohibit the formation of a quasi-spherical dome of at least 20 mm of height. Second, the highest limit of the regulation temperatures should not cause uncontrolled sagging nor excessive stretching of the HIPS sheet to avoid cracking of the speckle patterns or bursting the formed dome. As a result of this first calibration step, the selected regulation-temperatures corresponded to 270; 290; 310 and 330 °C.

The second step of calibration relied on qualitative and quantitative analyses of the distribution of the thermoplastic temperatures for each of the considered regulation temperatures and after the stabilization of the temperature of the IR heater. Thus, the evolution of the temperature of the HIPS sheet was recorded during a heating duration of 70 s that was followed by a cooling duration of almost one minute after the complete retraction of the IR heater. During this procedure the stretching step of the forming cycle was not activated. During each heating and cooling operation, temperatures were simultaneously recorded at four control positions using K-type

Table 2 Output of the calibration operation of the stereo-DIC system

		Camera 1 (right)		Camera 2 (left)	
Positions (mm)and orientations (°) of the cameras	X axis	13.3	22.5	−25.4	22.8
	Y axis	−24.8	17.3	−30.5	−17.7
	Z axis	997.9	0.8	994.9	−0.6
Size of dewarped image (pixel)	2109 × 2001				
Origin coordinates (pixel)	(1020.85; 965.986; 0)				
Scale factor (pixel/mm)	7.611				
Pixel aspect ratio	1				
Pixel size (μm)	5.5				
In-plane precision (pixel)	0.568				

thermocouples. The use of thermocouples was favored over the use of a thermal imaging camera because of the limited accessibility of the surface of HIPS sheets during radiative heating. A total of 42 control positions was tested to cover a domain of 100×120 mm^2 located at the center of the thermoplastic sheet and delimited by the contour Γ_{Krig} (Fig. 1a). The coordinates of these control positions were coincident with the nodes of a regular grid which was sketched on the initially flat surface of each the used HIPS samples. All recorded temperatures indicated a limited decrease of less than 5 °C during the first 5 s following the retraction of the IR-heater. Thus, during the stretching step which is limited to 1.5 s, it is assumed that the temperature variation was negligible. For a reason of clarity, only the temperatures recorded at the origin of the stereo-vision referential are reported in Fig. 3.

To qualitatively evaluate the susceptibility of the HIPS sheets to sag, measured temperatures were compared to the temperature of heat deflection T_{HD} (Table 1). In fact, the T_{HD} corresponds to a temperature threshold that marks the softening of a thermoplastic sample and the initiation of its deflection under a constant load during a heating cycle. In this study the local geometric stability of the softened sheet was evaluated by mapping the spatial distribution of temperature gaps θ_i defined in eq. (4):

$$\theta_i = T_i - T_{HD} \tag{4}$$

Where T_i is the temperature measured at the beginning of the stretching operation at a control position i.

Then, all evaluated temperature gaps at the considered control-positions were used as input to generate statistical maps based on the Kriging interpolation method using a spatial statistics toolbox *(EasyKrig v3.0)* [36] and the software *Matlab (MathWorks Inc., Natick, MA, USA)*.

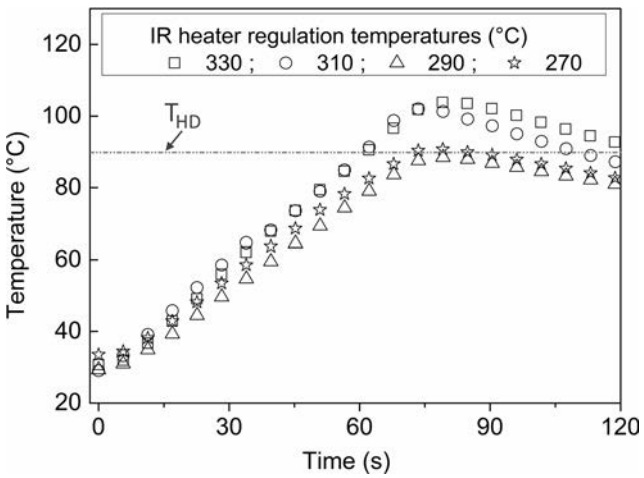

Fig. 3 Temperature profiles recorded at the origin of the considered stereo-vision referential (X, Y, Z) during a radiative heating operation of 70 s followed by cooling at room temperature

Stereo DIC computations

The software *DaVis v8.4* was used to post-process the pairs of stereo images that were recorded by conducting a total of five forming cycles for each of the considered four regulation temperatures of the IR heater. All stereo-DIC computations considered a circular field-of-view of 120 mm in radius that was concentric to the circular opening of clamping frame. A gap of 5 mm from the edge of the wooden clamp-frame was considered to avoid potential errors of the image-correlation computations that might be caused by local shadow zones of the clamp-frame on the surface. The used subset and the step-size corresponded respectively to 81×81 pixels and 21×21 pixels. Due to the large out-of-plane deformations of the softened HIPS sheets the *sum of the differential* method was considered to conduct the images-correlation computations in a Lagrangian coordiantes system [37]: It consisted on evaluating displacement vectors at a time increment t_n by summing all the elementary increments of displacement vectors evaluated between the time increments t_i *and* t_{i+1}. Where $i \in \{0, 1, 2, \ldots, n-1\}$ and t_0 corresponded to reference of times attributed to the reference state of image-correlation computations. In the current work, all correlation computations were performed accordingly to the framework of large strains by using the software DaVis and the same calibration parameters (Table 2). Because the aim of the current study is related to the reliability of the measured strains related to the choice of the reference state of correlation computations, reconstruction and correlation sources of error were assumed within the tolerance range of the calibrated stereo-DIC equipment and were not evaluated separately. The main focus was attributed to displacement vectors and major and minor principal Green-Lagrange strains as out-put of the image-correlation computations [38].

Because the stereo-vision measurements were only possible after softening the HIPS samples, the adopted approach consisted on evaluating pressure induced mechanical strains with consideration of two steps. The first step assumed that the reference of displacement vectors corresponded to the deformed speckle observed on the sagged surface at the moment of complete retraction of the IR heater. This assumption was required to qualitatively analyze the evolution of the out-of-plane components of displacement vectors (w) in order to get more insight about the damped out-of-plane oscillations associated with the transition from the sagged to the strained shapes of the softened HIPS sheet. The second step consisted on shifting the reference of displacement vectors to the moment of attenuation of the damped out-of-plane oscillations to evaluate pressure induced mechanical strain corresponding to a quasi-stable stretching regime of the sheet. The mathematical difference between strains from both sub-steps corresponds not only to the shift of the reference of image-correlation computations but also represents pressure induced

mechanical strains which are more dependent of the uncontrolled change of initial conditions caused by sag and warpage flaws. Thus, the global mechanical stain ε^{DIC} measured by stereo-DIC during the stretching operation with consideration of the sagged surface as a reference of image-correlation computations can be expressed as indicated in eq. (5):

$$\varepsilon^{DIC} = \varepsilon^{unst} + \varepsilon^{st} + o(\varepsilon^{st}) \quad (5)$$

Where, ε^{DIC} is the global stereo-DIC strain; ε^{unst} is the pressure induced mechanical strain during the attenuation of the damped oscillations; ε^{st} is the pressure induced mechanical strain after the attenuation of oscillations; and $o(\varepsilon^{st})$ is a mathematical function which represents the correlation and reconstruction errors.

Results and discussion

Susceptibility to surface planarity change

Figure 4 shows that for all the considered regulation temperatures, the corresponding maps of temperature gaps indicated non-homogeneous distributions at the start of the stretching operation. Moreover, the increase of the regulation temperature corresponded to an increase of thermal gradients in the direction of the X axis. With consideration of the automatic regulation of the temperature of the IR heater, such qualitative results confirmed a limited efficiency of the radiative heat transfer mode mostly caused by the change of the local orientations of the initially flat surface of the HIPS sheets [25, 33].

According to the statistical data provided in Table 3 two configurations of surface planarity changes were observed. The first configuration corresponded to the case of the lowest limit of regulation temperatures (270 °C). In fact, the predominance of negative temperature gaps indicated that the surface was rigid enough to resist any deflections caused by the gravitational force. Thus, the planarity changes in the control domain were caused by the relaxation of local residual stresses of the clamped HIPS sheet (Fig. 5a and b). Consequently, all inflation tests conducted at this thermal condition could be considered as reference tests of insignificant sag levels and of limited transitions of surface shapes during stretching. The second configuration corresponded to the cases where the average temperature gaps were positive ($avg(\theta_i) \geq 0^{\circ}C$). In these cases, the increase of the regulation temperature indicated a higher susceptibility of the softened samples to deflect (Fig. 5c and d).

Qualitative analyses of the transient surface deformations

In the first step of stereo-DIC computations, the reference state of displacement vectors was attributed to the pair of images of the speckle that corresponded to the onset moment of air inflation. The identification of this moment was based on the variation of the relative pressure signal which was

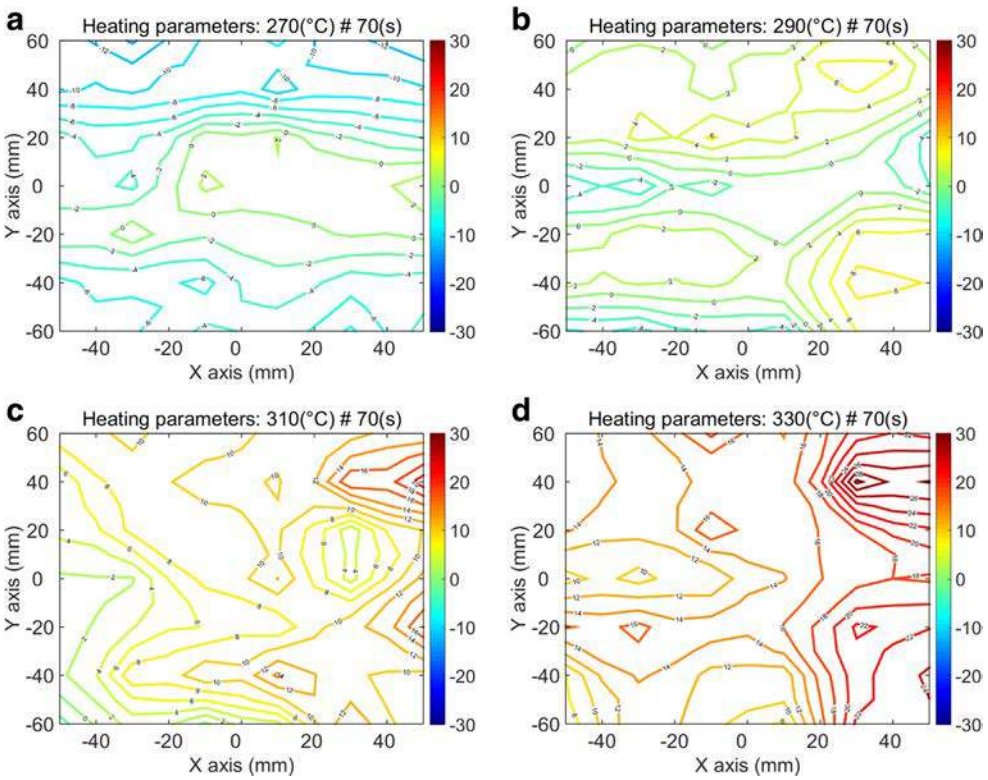

Fig. 4 Temperature maps generated based on the Kriging interpolation method. The maps (a), (b), (c) and (d) indicate the gaps between the heat deflection temperature and the HIPS sheet temperatures measured at the end of the 70s heating duration and conducted respectively at the regulation temperatures of 270, 290, 310 and 330 °C

Table 3 Statistical data of the calculated temperature gaps at the selected 42 control-positions

Heating parameters	Min	Max	Avg	Std
270 (°C) # 70 (s)	−14.3	3.6	−4.5	4.3
290 (°C) # 70 (s)	−6.7	9.2	1.6	3.7
310 (°C) # 70 (s)	−2.8	21.2	8.4	4.4
330 (°C) # 70 (s)	6.7	30.5	16.0	4.8

synchronized with the stereoscopic recording time (t) **(**Fig. 2**)**. Time evolution of average of *w* were calculated from displacements measured inside a virtual gauge of 20 × 20 mm^2 which was defined at the pole of each of the formed bubble and which corresponded to the contour Γ_P in Fig. 1**a.** All the obtained averages of *w* profiles of all the formed domes are illustrated in Fig. 6. The out-of-plane displacements at polar domains confirmed that the interaction between the pressurized-air and the softened surface passed by two successive regimes particularly for regulation temperatures higher than 270 °C. The first regime covered almost 300 ms from the start of the inflation operation and represented the duration required for the attenuation of damped out-of-plane oscillations of the sagged thermoplastic sheet. The second regime corresponded to the effective stretching of the softened HIPS sheets where *w* increased gradually until reaching a plateau indicating the end of the 1.5 s duration of inflation.

With the increase of the regulation-temperature of the IR heater, the first regime of interaction between the softened HIPS sheet and compressed-air was marked by the occurrence and the amplification of local displacement optimums (Fig. 7). The repetitiveness of the observed phenomena was confirmed for all the tests that corresponded to positive average of temperature gaps ($avg(\theta_i) \geq 0$). At first thought, the observed amplification of these local displacement optimums would be associated to an increase of the sag levels or even to the existence of some instabilities of the used experimental rig. However, the absence of the observed local optimums at the lowest regulation temperature (270 °C), confirmed that the observed phenomenon was related to an amplification of the pressure induced surface oscillations due to sagging confirmedly to the qualitative results of the maps of temperature gaps θ (Fig. 4).

Identification of the effective reference for stereo-DIC computations

To shade more light on the observed local displacement optimums at the polar domains, the time derivatives of the out-of-plane displacements during the first stretching domain were evaluated. With respect of the used image recording frequency of 180 Hz and the duration of inflation operations (1.5 s) the derivatives of displacements could be expressed in a discretized form as indicated in eq. (6):

$$\frac{\partial w}{\partial t} = \lim_{t_{i+1} \to t_i} \left(\frac{w_{i+1} - w_i}{t_{i+1} - t_i} \right) \cong \frac{(w_{i+1} - w_i)}{1/180} \tag{6}$$

Where *w* and *t* indicate respectively the average of out-of-plane components of the displacement vectors and time increment corresponding to the two successive stereoscopic-image pairs of the incremental orders *i* and *i + 1*.

Figure 7a represents the time evolution of the calculated out-of-plane displacements and their corresponding derivatives (which is equivalent to a velocity) in the case of the

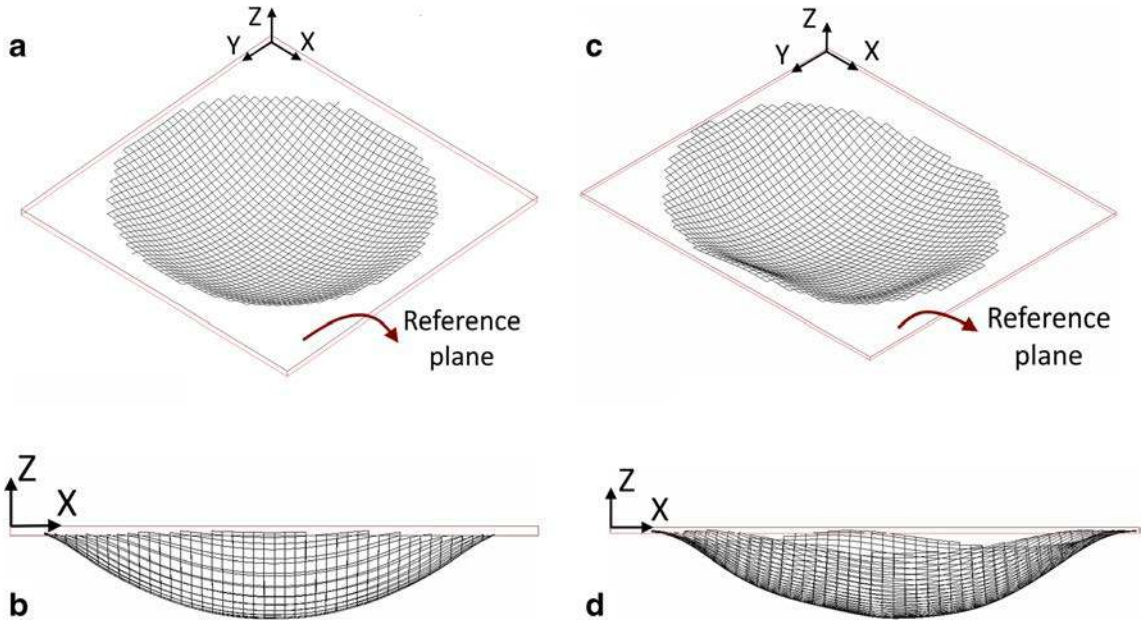

Fig. 5 Isotropic and side views of 3D geometric changes due to warpage (a-b) and sagging (c-d) at the end of two different heating steps

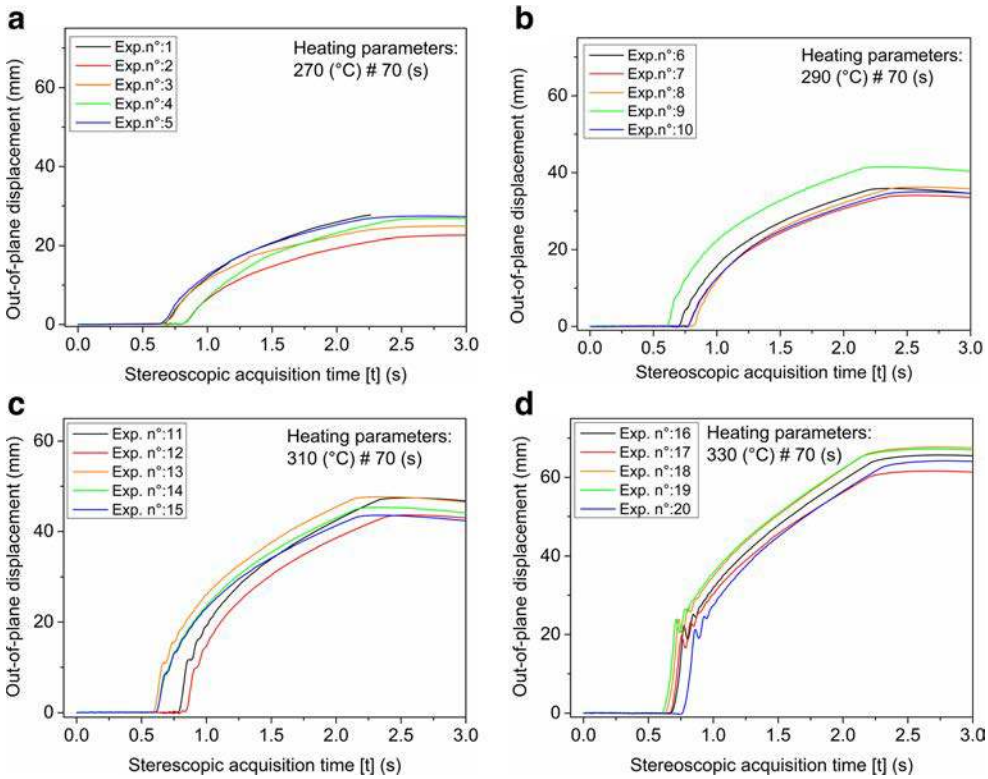

Fig. 6 Out-of-plane displacement obtained from the step 1 of the image-correlation computations at the polar domain of the performed stretching tests at the regulation temperature of **a** 270 °C, **b** 290 °C, **c** 310 °C and **d** 330 °C

stretching test of the reference Exp.n°20 that was conducted at the regulation temperature of 330 °C. As observed the alternation between local maxima and minima of the derivative corresponded to the inflection points of out-of-plane displacements. Despite the previous observation was mathematically evident, it physically reflects a pressure jump at the initiation of the stretching step and a more and more significant sagging of the sheet which is caused by a combination of gravity force and increasing viscous of the thermoplastic during the precedent heating step (Fig. 2).

Based on the damped time-evolution of the derivative of displacements, a decayed exponential expression as indicated by eq. (7) was considered to fit the time-decrease of the corresponding local maxima.

$$a = a_0 + \alpha \times exp\left[-\frac{(t-t_0)}{\tau}\right] \tag{7}$$

Where: t_0, a_0, α and τ respectively referred to a time offset, an amplitude offset, a pre-exponential coefficient and characteristic time duration.

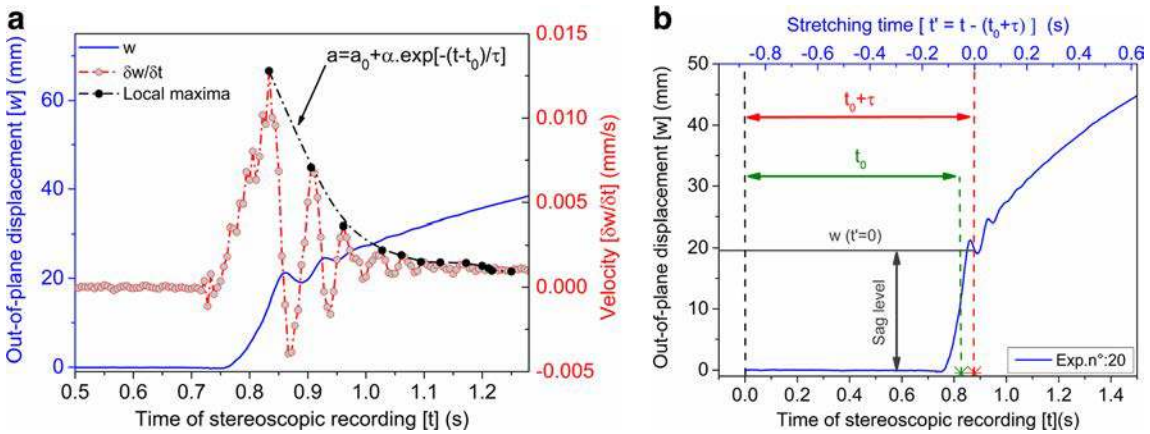

Fig. 7 **a** Time evolution of the derivative of the out-plane displacement corresponding to the test of the reference Exp. n°20 conducted at the heating parameters 330 (°C) # 70 (s). **b** Graphical representation of the considered time-shift corresponding to the attenuation of 63% of the out-of-plane transient effects which take place during the transition from the sagged to the strained shapes of the HIPS sample of the reference Exp.n°20

The advantage of using of a decayed exponential form is related to the significance of the characteristic time duration ($t = t_0 + \tau$) which corresponds to the duration required for the attenuation of 63% of the maximal velocity amplitude $\left(\frac{a-a_0}{\alpha}\right)_{|t=t_0}$ at the origin of inflation times. The derivation and fitting operations were extended to all the conducted inflation tests including those conducted at the lowest regulation temperature (270 °C) that were considered as reference tests of negligible sag levels.

Table 4 shows that the characteristic-times (τ) relative to bubble-inflation tests which were conducted at similar thermal conditions presented relatively similar orders of magnitude. Consequently, regardless of the dependence of the initial sag level of the thermal conditions, τ represented an indicator of the moment of attenuation of about 63% of the damped oscillations (Fig. 7b) and which corresponded to the moment of initiation of effective stretching of the softened thermoplastic sheet. The identified characteristic times (τ) were then used to shift the reference of displacement vectors to conduct the second step of stereo-DIC computations. In this context, a time-shift from the origin of the inflation operation was considered to define the effective stretching time (t') as indicated in eq. (8):

$$t' = t - (t_0 + \tau) \tag{8}$$

Figure 8 shows the obtained out-of-plane displacements obtained from the second step of image correlation computations. With consideration of the shifted reference of displacement vectors, the softened sheets indicated different sag levels even for the tests conducted after similar heating operations. However, the observed local optimums were superposed mostly in the regulation temperatures of 290; 310 and 330 °C.

Sag level and amplification of damped sheet oscillations

To provide more insight about the interactions which took place between the softened thermoplastic sheet and pressurized-air, two representative cases were considered to illustrate the transition of the surface shapes respectively after warpage and sag. The surface shapes were reconstituted at each time-increment from the deformed meshes of the virtual gauges which were used to evaluate displacement vectors. The corresponding image-correlation computations were conducted starting from the sagged shape of the surface until reaching the onset of the effective stretching regime (t' = 0). To illustrate the attenuation of surface oscillations, the reference of surface deformations was also attributed to the images corresponding to t' = 0.

In the case of warpage (Fig. 9) the evolution of the projections of the surface shape in the (YZ) plane were not symmetric and showed increasing out-of-plane displacements with no presence of local optimums confirmedly to the previous observations at the polar domain observed during the first regime

Table 4 Identified parameters using eq. (2) and corresponding dimensionless sag

Regulation temperature (°C)	Exp.n:	a_0 (mm/s)	α (mm/s)	t_0 (s)	τ (s)	Σ(−)
270	1	6.79	40.16	0.73	0.38	0.116
	2	5.67	24.12	0.96	0.34	0.095
	3	5.31	34.58	0.78	0.33	0.107
	4	6.48	42.22	0.81	0.41	0.100
	5	5.62	37.74	0.71	0.4	0.119
290	6	10.23	97.68	0.69	0.28	0.118
	7	9.93	72	0.75	0.28	0.108
	8	9.69	76.66	0.81	0.3	0.128
	9	11.19	103.63	0.61	0.3	0.156
	10	9.12	70.07	0.77	0.29	0.116
310	11	13.64	127.91	0.74	0.22	0.133
	12	12.03	125.81	0.79	0.22	0.123
	13	14.02	137.47	0.56	0.2	0.127
	14	15.12	126.17	0.56	0.21	0.114
	15	14.12	132.5	0.55	0.21	0.106
330	16	27.59	370.77	0.75	0.05	0.151
	17	24.95	305.37	0.71	0.07	0.133
	18	28.47	388.12	0.7	0.05	0.164
	19	27.77	347.01	0.68	0.05	0.164
	20	27.22	334.63	0.83	0.05	0.157

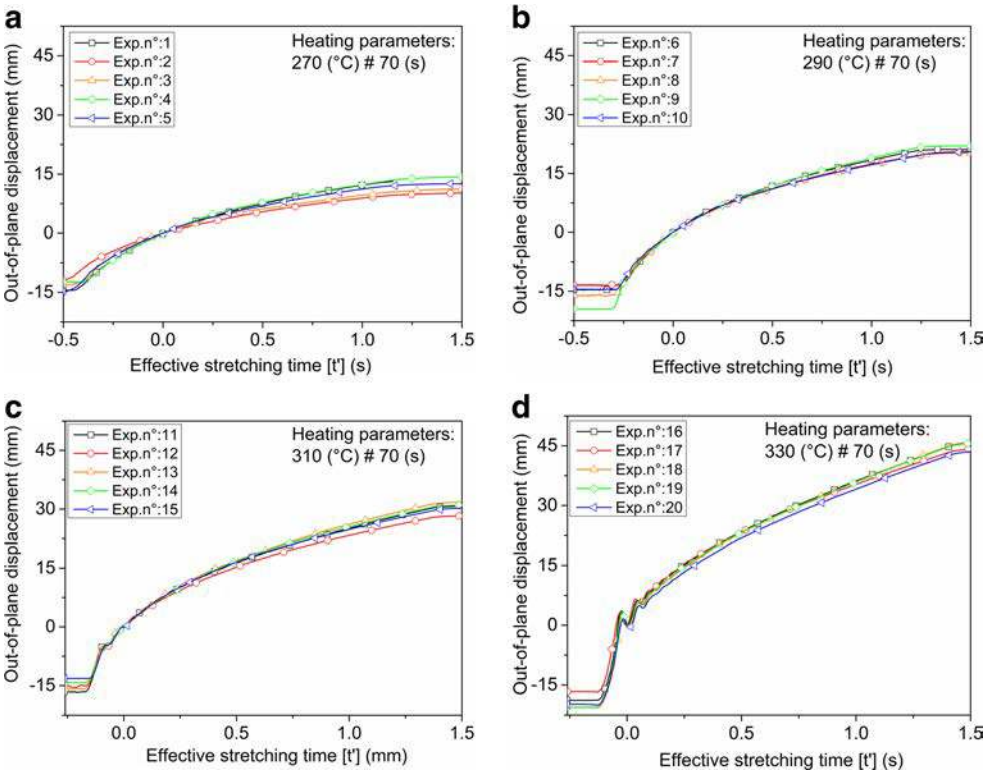

Fig. 8 Out-of-plane displacement obtained from the step 2 of the image-correlation computations at the polar domain of the preformed stretching tests at the regulation temperature of **a** 270 °C, **b** 290 °C, **c** 310 °C and **d** 330 °C

of stretching. In the case of the sagged surface (Fig. 10) the projections of the surface shape in the (YZ) plane were marked by an alternation of the maximum out-of-plane displacements between the center of the sheet located at (Y = 0) and two other regions symmetrically positioned around Y = 70 mm and Y = −70 mm. With consideration of the shape factor of the used HIPS samples of 1.8 and the distribution of temperature gaps, the observed changes of surface shape after sag were not random, rather they were symmetrical via the plane (XY).

To quantitatively analyze the variation of sag levels under the studied regulation temperatures, dimensionless sag levels were calculated based on eq. (9):

$$\Sigma = \frac{\left|w(t=0) - w\left(t' = 0\right)\right|}{r_0} \tag{9}$$

Where $w(t = 0)$ is the maximum out-of-plane displacement of the sagged surface, $w(t' = 0)$ is the surface out-of-plane displacement after the attenuation of 63% of the transient displacements and r_0 is the radius of the formed bubbles (125 mm).

Figure 11 shows that within the tested thermal conditions, the increase of dimensionless sag (Σ) corresponded to a decrease of the characteristic times. The scatter of the distribution of temperature gaps (θ), induced also a scattered distribution of Σ. However, the corresponding characteristic times were relatively more homogeneous particularly for the positive averages of temperature gaps. These results indicated that under similar radiative heating conditions, the measured sag levels were sensitive to the local temperature distributions. Nevertheless, the variation of the characteristic times (τ) indicated that the velocity of the sagged sheets during stretching was more affected by the change of the regulation temperature rather than the local temperature distributions at the surface of the HIPS sheet.

Evaluation of mechanical strains during the stretching step: case of application

In this section, the stretching test of the corresponding references Exp.n°1, Exp.n°6, Exp.n°11 and Exp.n°16 were considered. For each of the considered tests, two reference states were defined: the initial reference state corresponded to the sagged shape of the sheet at the initiation of the stretching step and the second reference state was defined based on a time shift based on velocity characteristic-time in Table 4. Displacement vectors and both major and minor principal mechanical strains on the surface of the formed bubbles were evaluated according to the same image-correlation procedure previously indicated in section 2.4. ε_1^{DIC} and ε_1^{st} (respectively ε_2^{DIC} and ε_2^{st}) represent the evaluated major (respectively minor) principal strains before and after shifting the reference state of the correlation computations. To compare between the different correlation results a fixed pressure level of 385 Pa was considered.

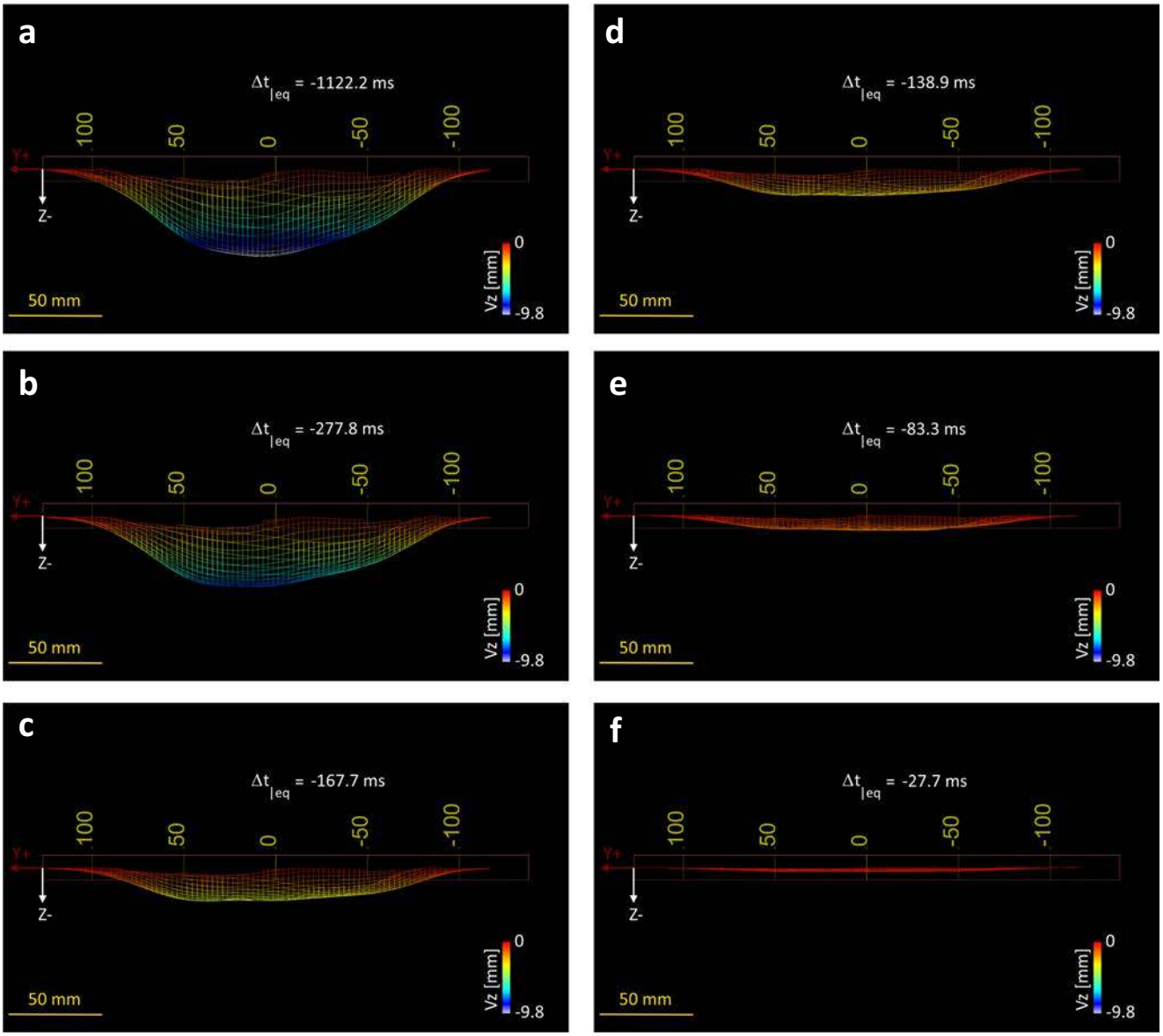

Fig. 9 Time evolution of the shape of the sheet during the initial regime of stretching of the HIPS sheet of the reference Exp. n°:1 after being conditioned at the heating parameters 270 (°C) # 70 (s). To highlight the out-of-plane changes the regenerated meshes were stretched by applying a multiplicative factor of 10 only in the Z direction (indicated by the white arrow)

Figure 12 illustrates the out-of-plane displacements of the material points located along the diameter (at Y = 0) of the Ω_{sag} domains after shifting the reference of correlation computations to the moments of attenuation of 63% of the velocity amplitudes. The achieved maximum surface heights corresponded to 21.4%, 25.9%, 32.7% and 44.3% of the bubble radius of 125 mm and they are all within the calibration domain of the stereo-DIC equipment. The semi-spherical shapes indicate that sheet at the considered pressure level was not subjected to any catastrophic stretching. For simplification reasons the term $o(\varepsilon^{st})$ attributed to reconstruction and correlation sources of error in eq. (5) is not considered.

As shown in Figs. 13 and 14, the calculated minor and major principal components of global ε_q^{DIC} and quasi-static ε_{qi}^{st} mechanical strains during step 1 and step 2 respectively indicated an increase of the strain levels at the considered pressure level (of 385 Pa) with an increase of regulation temperatures. Moreover, with consideration of the evaluated maps of temperature gaps at the center of the stretched sheets the evolution of minor and major strain levels after filtering the damped out-of-plane oscillations presented also local gradients along the X axis for the regulation temperatures of 310 and 330 °C. Complementarily, the zones of localization of the highest major principal strains corresponded to the zones of the highest temperature gaps.

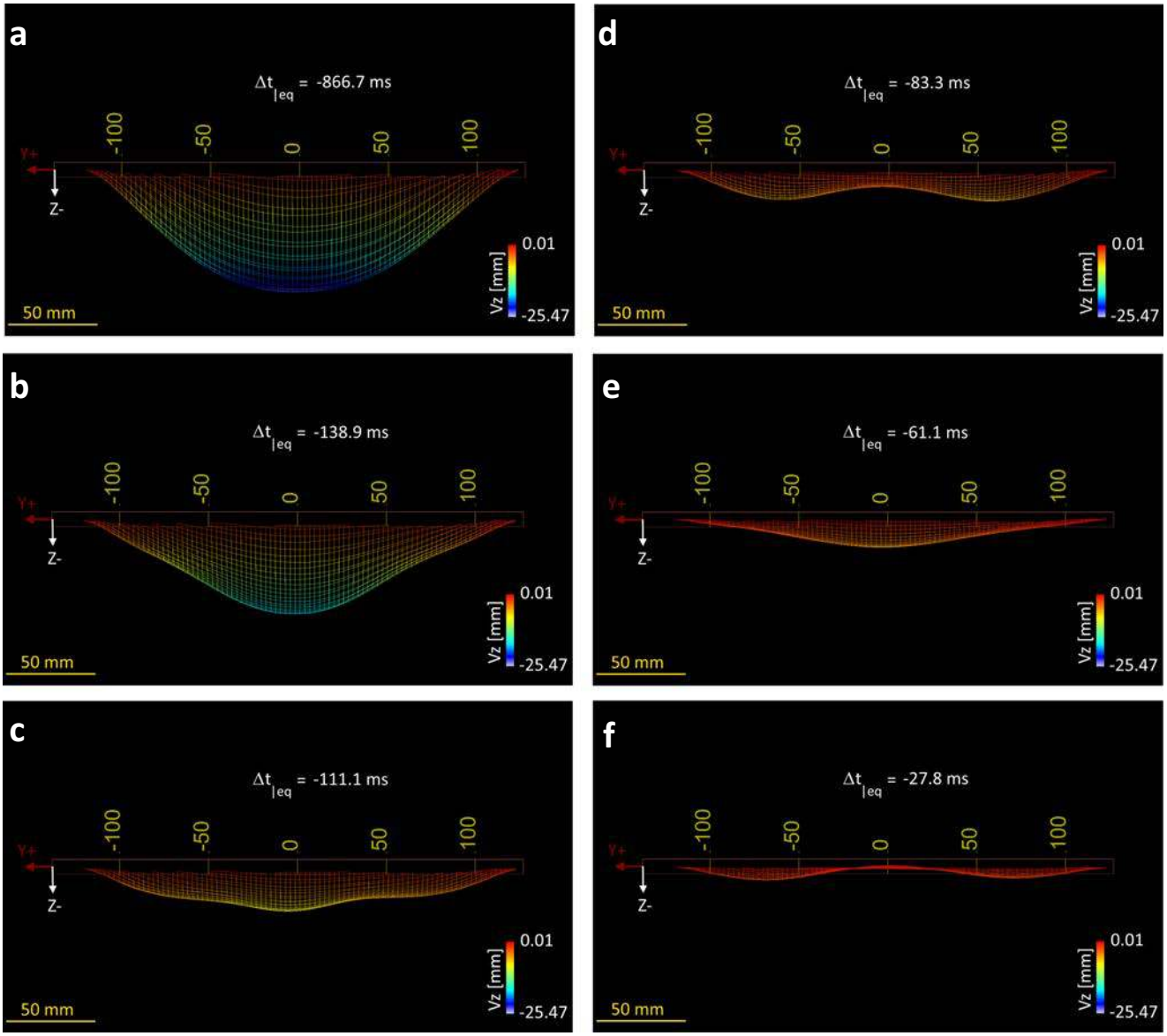

Fig. 10 Time evolution of the shape of the sheet during the initial regime of stretching of the HIPS sheet of the reference Exp. n°:20 after being conditioned at the heating parameters 330 (°C) # 70 (s). To highlight the out-of-plane changes the regenerated meshes were stretched by applying a multiplicative factor of 5 only in the Z direction (indicated by the white arrow)

A home-developed *Matlab* routine was then used to extract and match the spatial coordinates of the nodes of the meshes of both image-correlation computations. Then, for each of the matched nodes i of the coordinates $(x_i; y_i)$ a scalar β_i was calculated as indicated in eq. (10):

$$\beta_i = 100 \times \left| \frac{\varepsilon_{qi}^{DIC} - \varepsilon_{qi}^{st}}{\varepsilon_{qi}^{DIC}} \right| \quad i \in \{1, 2, \ldots, n\} \text{ and } q \in \{1, 2\} \tag{10}$$

Where,

n the total number of computing nodes;

ε_{1i}^{DIC} and ε_{2i}^{DIC} represent the major and minor principal strains on the surface of the sheet before shifting the reference state;

ε_{1i}^{st} and ε_{2i}^{st} represent the major and minor principal strains on the surface of the sheet after shifting the reference state.

Each scalar represented the local fraction of ε_{qi}^{unst} strains, which is affected by the uncontrolled change of local thermal and geometric conditions taking place during the heating step. The median of overall calculated β_i scalars were then considered as a collective measurement

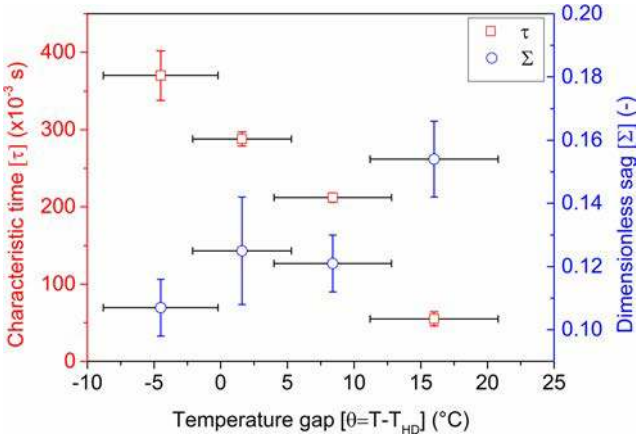

Fig. 11 Variation of the calculated average characteristic times and the corresponding average dimensionless sag under the effect of the measured temperature gaps

to statistically quantify the inaccuracy level of evaluated strains if a shift of the reference state would not be considered. In fact, the median was preferred over the average because the latter is more sensitive to local imprecisions which can be related to the correlation errors at the edges of the considered virtual gauge or to an excessive distortion of the corresponding mesh due to large deformations of the speckle [39]. The median of $\tilde{\beta}_q$ was defined based on eq. (11):

$$\tilde{\beta}_q = median\ of\ \{\beta_{q1}, \beta_{q2}, \ldots, \beta_{qn}\} \tag{11}$$

The evaluated medians $\tilde{\beta}_2$ were at least two times higher than $\tilde{\beta}_1$ and decreased with the increase of the sag levels. Indeed, in the case of the lowest regulation temperature (270 °C), $\tilde{\beta}_2$ was equal to 35.97% and $\tilde{\beta}_1$ was equal to

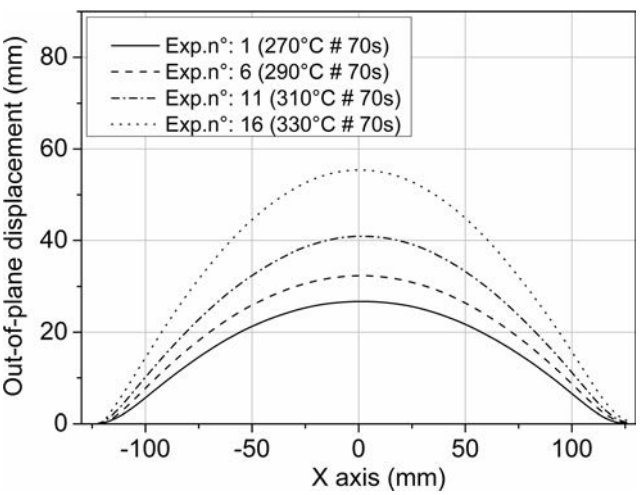

Fig. 12 Bubble shapes evaluated from the step 2 of image correlation computations of the representative tests of the tested regulation temperatures and corresponding to the relative pressure of 385 Pa

14.88%, whereas for the highest regulation temperature (330 °C) the corresponding values were respectively equal to 15.47% and 4.49%. These results indicated that pressure induced mechanical strains are the least accurate when the surface changes are caused by warpage and that the increasing sag levels decreased the inaccuracy level related to the shift of the reference state of correlations.

According to the adapted identification method of the reference of the images-correlation calculations after heating the surface of the material, all the calculated scalars $\beta_1$and β_2 represented not only the strain imprecisions caused by variation of the thermal level but also imprecisions related to an amplification of the damped oscillation caused by an increase of the sagging level. Thus, strain fields evaluated from step 2 of stereo-DIC computations were more representative of the effective stretching of the material as they considered an attenuation of 63% of transient geometric non linearity independently of the considered thermal level.

Conclusions

The dependence of the reference of image-correlation computations of uncontrolled the change of initial conditions was investigated during stretching HIPS sheets after warpage and sag. Different sag levels were regenerated based on an experimental rig and by mapping gaps between measured and heat deflection temperatures. To identify the references of image-correlation computations a two-step procedure was proposed and tested at four different heating conditions.

In the first step of this procedure, out-of-plane displacements were qualitatively evaluated by defining the sagged shape of the sheet as the reference of displacements. Based on the damped time-evolution of the displacement derivatives, temperature-dependent characteristic times were then determined using a decayed exponential time expression. These characteristic times marked the transition between two regimes of the interaction between the inflated air and the softened HIPS sheet. The first regime corresponded to the occurrence of damped surface undulations. These shape changes presented an axial symmetry with the increase of sag levels. The second regime corresponded to the effective stretching of the softened HIPS sheet starting from the moment of attenuation of the damped out-of-lane undulations.

In the second step of the procedure, strain fields were computed by attributing the reference of image-correlation computations to the moment corresponding to the attenuation of 63% of the initial sag amplitudes. To demonstrate the effectiveness of the procedure, an application case at a constant relative pressure of 385 Pa was considered to evaluate inaccuracy levels of principal strains at four thermal conditions. The obtained results indicated higher median inaccuracy levels of minor principal strain fields than major principal

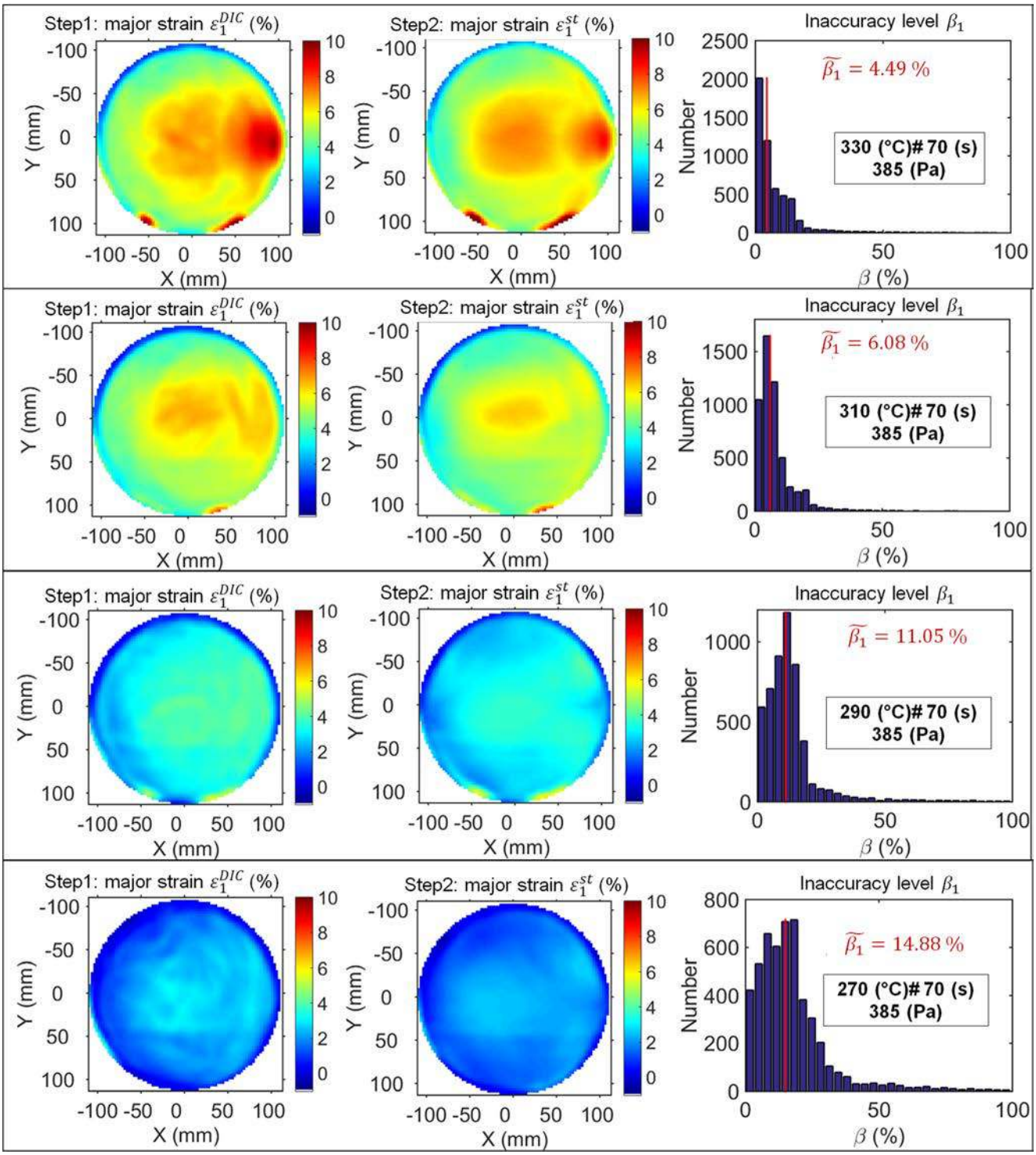

Fig. 13 Major principal strains evaluated by the proposed two-step approach and the median degree of inaccuracy corresponding to each of tested regulation temperatures

strain fields and that the increase of the sag level induced the decrease of the corresponding median inaccuracy levels. These results indicated a higher reliability of the suggested method when surface shape transitions were caused by sag. It was shown also that the developed approach provides an experimental methodology to extend the use of stereo DIC measurements in the context of thermoforming conditions of thermoplastic sheets particularly when the thermal deformations cannot be evaluated during heating.

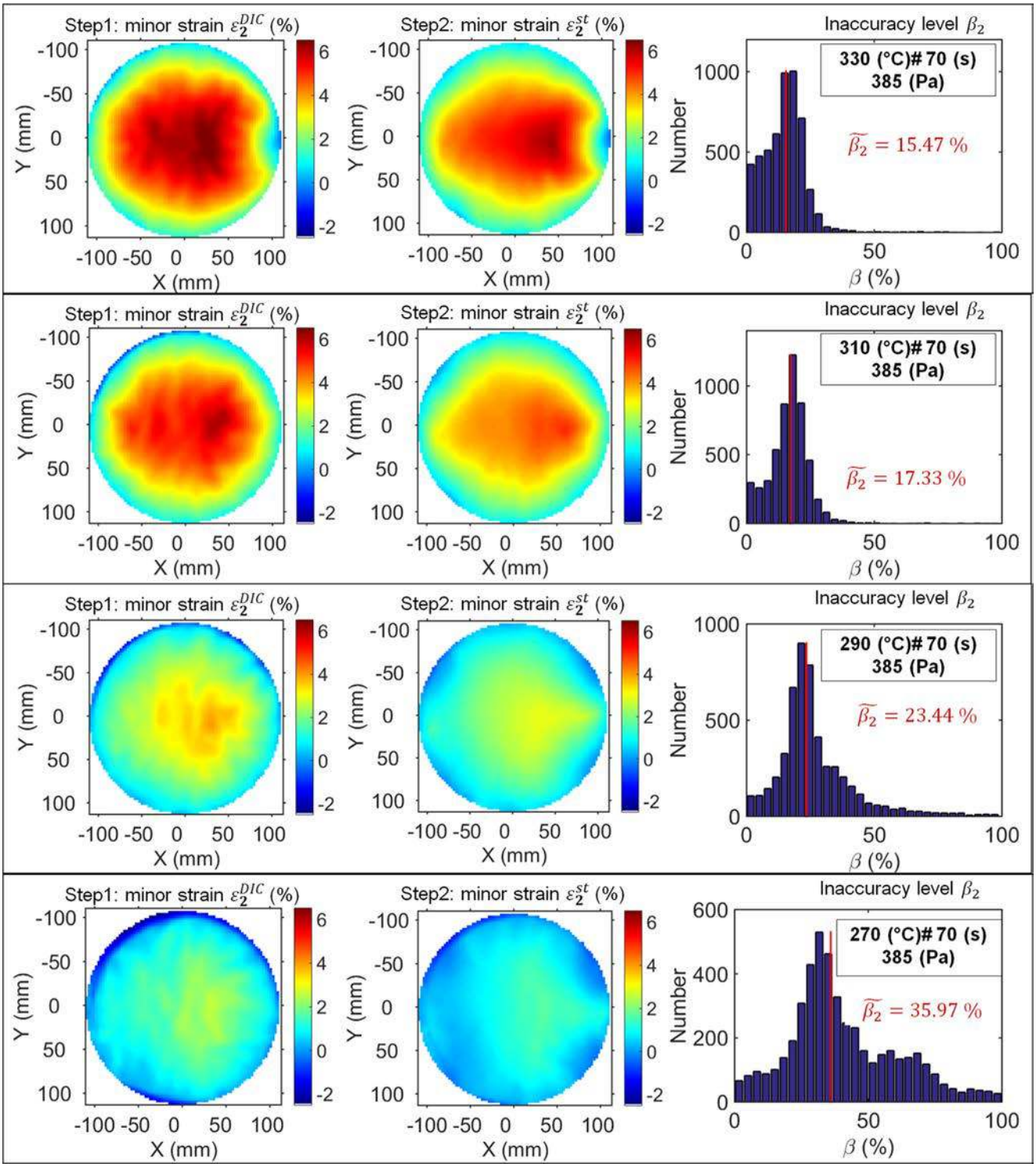

Fig. 14 Minor principal strains evaluated by the proposed two-step approach and the median degree of inaccuracy corresponding to each of tested regulation temperatures

Acknowledgements The authors acknowledge the European Union (European Regional Development Fund FEDER), the French state and the Hauts-de-France Region council for co-funding the ELSAT 2020 by CISIT project (POPCOM action).

Compliance with ethical standards

Conflict of interest The authors declare that they have no conflict of interest.

References

1. Ayadi A, Lacrampe M-F, Krawczak P (2018) A comprehensive study of bubble inflation in vacuum- assisted thermoforming based on whole-field strain measurements. In: AIP Conference Proceedings 1960. American Institute of Physics
2. Leite W, Campos Rubio J, Mata Cabrera F et al (2018) Vacuum thermoforming process: an approach to modeling and optimization using artificial neural networks. Polymers (Basel) 10:143. https://doi.org/10.3390/polym10020143
3. Yoo YG, Lee HS (2011) Effects of processing conditions on thickness distribution for a laminated film during vacuum-assisted thermoforming. Trans Mater Process 20:250–256. https://doi.org/10.5228/KSTP.2011.20.3.250
4. Sasimowski E (2017) A pressure-bubble vacuum forming process for polystyrene sheet. Adv Sci Technol Res J 11:180–186. https://doi.org/10.12913/22998624/70801
5. Jenkins CH (1996) Nonlinear dynamic response of membranes: State of the art - Update. Appl Mech Rev 49:S41. https://doi.org/10.1115/1.3101975
6. Jenkins CH, Leonard JW (1991) Nonlinear dynamic response of membranes : State of the art. Am Soc Mech Eng 44:319–328. https://doi.org/10.1115/1.3101975
7. Machado G, Favier D, Chagnon G (2012) Membrane curvatures and stress-strain full fields of axisymmetric bulge tests from 3D-DIC measurements. Theory and validation on virtual and experimental results. Exp Mech 52:865–880. https://doi.org/10.1007/s11340-011-9571-3
8. Lăzărescu L, Nicodim I, Ciobanu I et al (2013) Determination of material parameters of sheet metals using the hydraulic bulge test. Acta Metall Slovaca 19:4–12. https://doi.org/10.12776/ams.v19i1.81
9. Patil A, Dasgupta A (2013) Finite inflation of an initially stretched hyperelastic circular membrane. Eur J Mech A/Solids 41:28–36. https://doi.org/10.1016/j.euromechsol.2013.02.007
10. Kumar N, Dasgupta A (2013) On the contact problem of an inflated spherical hyperelastic membrane. Int J Non Linear Mech 57:130–139. https://doi.org/10.1016/j.ijnonlinmec.2013.06.015
11. Cosola E, Genovese K, Lamberti L, Pappalettere C (2008) A general framework for identification of hyper-elastic membranes with moiré techniques and multi-point simulated annealing. Int J Solids Struct 45:6074–6099. https://doi.org/10.1016/j.ijsolstr.2008.07.019
12. Verron E, Khayat RE, Derdouri A, Peseux B (1999) Dynamic inflation of hyperelastic spherical membranes. J Rheol (N Y N Y) 43:1083–1097. https://doi.org/10.1122/1.551017
13. Verron E, Marckmann G, Peseux B, et al (2016) Dynamic inflation of non-linear elastic and viscoelastic rubberlike membranes To cite this version
14. Hild F, Roux S (2006) Digital image correlation: from displacement measurement to identification of elastic properties - a review. Strain 42:69–80. https://doi.org/10.1111/j.1475-1305.2006.00258.x
15. Palanca M, Tozzi G, Cristofolini L (2016) The use of digital image correlation in the biomechanical area: A review. Int Biomech 3:1–21. https://doi.org/10.1080/23335432.2015.1117395
16. Shao X, Dai X, Chen Z et al (2016) Calibration of stereo-digital image correlation for deformation measurement of large engineering components. Meas Sci Technol 27:125010. https://doi.org/10.1088/0957-0233/27/12/125010
17. Zappa E, Matinmanesh A, Mazzoleni P (2014) Evaluation and improvement of digital image correlation uncertainty in dynamic conditions. Opt Lasers Eng 59:82–92. https://doi.org/10.1016/j.optlaseng.2014.03.007
18. Duchene P, Chaki S, Ayadi A, Krawczak P (2018) A review of non-destructive techniques used for mechanical damage assessment in polymer composites. J Mater Sci 53:7915–7938. https://doi.org/10.1007/s10853-018-2045-6
19. Van Mieghem B, Desplentere F, Van Bael A, Ivens J (2015) Improvements in thermoforming simulation by use of 3D digital image correlation. Express Polym Lett 9:119–128. https://doi.org/10.3144/expresspolymlett.2015.13
20. Van Mieghem B, Lava P, Debruyne D et al (2013) Digital image correlation for on-line wall thickness measurements in thick gauge thermoforming. Key Eng Mater 554–557:1583–1591. https://doi.org/10.4028/www.scientific.net/KEM.554-557.1583
21. Van Mieghem B, Ivens J, Van Bael A (2016) Consistency of strain fields and thickness distributions in thermoforming experiments through stereo DIC. Exp Tech 40:1409–1420. https://doi.org/10.1007/s40799-016-0143-4
22. Li Y, Nemes JA, Derdouri AA (2001) Membrane inflation of polymeric materials: Experiments and finite element simulations. Polym Eng Sci 41:1399–1412. https://doi.org/10.1002/pen.10840
23. Hosseini H, Berdyshev BV, Mehrabani-Zeinabad A (2006) A solution for warpage in polymeric products by plug-assisted thermoforming. Eur Polym J 42:1836–1843. https://doi.org/10.1016/j.eurpolymj.2006.03.020
24. Kurtaran H, Erzurumlu T (2006) Efficient warpage optimization of thin shell plastic parts using response surface methodology and genetic algorithm. Int J Adv Manuf Technol 27:468–472. https://doi.org/10.1007/s00170-004-2321-2
25. Throne JL (2006) The effect of sheet sag on radiant energy transmission in thermoforming. Thermoforming Q 25:19–24
26. Giacomin AJ, Mix AW, Mahmood O (2010) Sag in thermoforming. Polym Eng Sci 50:2060–2068. https://doi.org/10.1002/pen.21734
27. Baek HM, Giacomin AJ, Wurz MJ (2014) Sag in commercial thermoforming. AIChE J 60:1529–1535. https://doi.org/10.1002/aic.14275
28. Murienne BJ, Nguyen TD (2016) A comparison of 2D and 3D digital image correlation for a membrane under inflation. Opt Lasers Eng 77:92–99. https://doi.org/10.1016/j.optlaseng.2015.07.013
29. Sutton MA, Yan JH, Tiwari V et al (2008) The effect of out-of-plane motion on 2D and 3D digital image correlation measurements. Opt Lasers Eng 46:746–757. https://doi.org/10.1016/j.optlaseng.2008.05.005
30. Ke X-D, Schreier HW, Sutton MA, Wang YQ (2011) Error assessment in stereo-based deformation measurements. Exp Mech 51:423–441. https://doi.org/10.1007/s11340-010-9450-3
31. Niu Y, Pham VL, Wang J, Park S (2018) An accurate experimental determination of effective strain for heterogeneous electronic packages with digital image correlation method. IEEE Trans Components, Packag Manuf Technol 8:678–688. https://doi.org/10.1109/TCPMT.2018.2794505
32. Rokoš O, Hoefnagels JPM, Peerlings RHJ, Geers MGD (2018) On micromechanical parameter identification with integrated DIC and the role of accuracy in kinematic boundary conditions. Int J Solids Struct 146:241–259. https://doi.org/10.1016/j.ijsolstr.2018.04.004
33. Buffel B, Amerijckx M, Hamblok M et al (2015) Experimental and computational analysis of the heating step during thermoforming of thermoplastics. Key Eng Mater:651–653. https://doi.org/10.4028/www.scientific.net/KEM.651-653.1003
34. Schmidt FM, Le Maoult Y, Monteix S (2003) Modelling of infrared heating of thermoplastic sheet used in thermoforming process. J

Mater Process Technol 143–144:225–231. https://doi.org/10.1016/S0924-0136(03)00291-7
35. Wang Z, Kieu H, Nguyen H, Le M (2014) Digital image correlation in experimental mechanics and image registration in computer vision: Similarities, differences and complements. Opt Lasers Eng 65: 18–27. https://doi.org/10.1016/j.optlaseng.2014.04.002
36. Selvadurai APS, Selvadurai PA (2010) Surface permeability tests: experiments and modelling for estimating effective permeability. Proc R Soc A Math Phys Eng Sci 466:2819–2846. https://doi.org/10.1098/rspa.2009.0475
37. Pottier T, Vacher P, Toussaint F et al (2012) Out-of-plane testing procedure for inverse identification purpose: application in sheet metal plasticity. Exp Mech 52:951–963. https://doi.org/10.1007/s11340-011-9555-3
38. LaVision stereo-DIC manuals (2016) Advanced digital image correlation systems for optical full field measurement of material strain, displacement and shape. https://www.lavision.de
39. Liu W, Long R (2015) Constructing continuous strain and stress fields from spatially discrete displacement data in soft materials. J Appl Mech 83:011006. https://doi.org/10.1115/1.4031763